# CLASSIFICATION OF GAIT ANOMALIES BY USING SPACE-TIME PARAMETERS OBTAINED WITH POSE ESTIMATION

STALIN BENENAULA $^1,$  MILTON DAMIAN TRELLES $^1$ LUIS EDUARDO GARZA-CASTAÑÓN $^2$  AND LUIS ISMAEL MINCHALA $^{1,2,*}$ 

 $^{1}\mbox{Department}$  of Electrical, Electronics and Telecommunications Engineering Universidad de Cuenca

Ave. 12 de Abril y Agustin Cueva, Cuenca 010101, Ecuador { stalin.benenaula; damian.trelles }@ucuenca.edu.ec \*Corresponding author: ismael.minchala@ucuenca.edu.ec

<sup>2</sup>School of Engineering and Sciences Tecnologico de Monterrey Av. Eugenio Garza Sada 2501 Col. Tecnológico C.P. 64700, Monterrey, Nuevo León, México legarza@tec.mx

Received April 2022; revised August 2022

ABSTRACT. Identifying anomalies in people suffering from gait disorders is typically performed by invasive methods, which implies attaching equipment to the human body. For instance, electromyography, as well as the use of body markers, are tools used to evaluate pathological gaits. This work presents a non-invasive system for analyzing and classifying normal, hemiparetic, and paraparetic gaits. To this end, we combine computer vision algorithms and artificial intelligence to generate space-time parameters related to the lower limbs' movement. The proposed methodology consists of capturing RGB images of volunteers that perform several cycles of the normal, hemiparetic, and paraparetic gaits. Pose estimation models process these images, and intelligent classifiers, based on convolutional neural networks (CNN) and support vector machine (SVM), and process skeleton gait energy image (SGEI) to achieve characterization and classification of gait, respectively. From the three gait patterns, it is obtained of stride length, cadence, stride width, stride time, gait speed, and angles of the body's lower extremities. Experimental results show high efficiency in the gait pattern classification, with efficiencies up to 98.57%.

Keywords: Artificial intelligence, Classification, Gait anomalies, Image processing

1. Introduction. Nowadays, the study of conditions that degenerate the mobility of the skeletal-muscular system constitutes a great concern of modern science. Alterations in the gait pattern imply pathological gaits requiring monitoring, control, and appropriate identification to guide neuro-physical rehabilitation processes. The most common causes of gait disorders are brain damage and traumatic injuries. These conditions produce pathological gaits such as hemiparetic and paraparetic.

Studying gait patterns using invasive and uncomfortable tools attached to the body, such as electromyography or body markers, is standard practice [1]. Nevertheless, there are also user-friendly approaches to studying gait; for instance, RGB-D sensors such as the *Kinect* [2], which is not invasive but could be expensive and difficult to acquire [3]. Body markers are used in [4] to estimate the poses of 28 patients with impaired sagittal balance. The authors analyze and evaluate this pathological gait through space-time parameters and kinematics of the gait. [5] analyzes and classifies gait anomalies using an RGB-D device. Upper and lower body movement is used as a gait characterization method, while

DOI: 10.24507/ijicic.18.06.1913

an SVM algorithm classifies normal gait from impaired gait. Experimental results show a classification accuracy of 85.87%. These two studies analyze pathological gaits using the *Kinect* device or body markers, which commits the patient to a laboratory environment for data collection.

As previously discussed, developing non-invasive systems for studying gait impairments is essential. There are some research papers on this matter; for instance, [6] focuses on classifying pathological gaits, such as diplegic, neuropathic or parkinsonian, by using gait energy image (GEI) [7], based on the sagittal movement of the body silhouette during walking. The combination of GEI and CNN allowed a precision in classification up to 89.6%. Our work compares the efficiency in classifying two pathological gait patterns and normal gait by using the pose estimation models OpenPose and PoseNet, which require RGB videos as input. There are reports of these pose estimation models in health-related applications. For instance, the authors of [8] use OpenPose to estimate various spacetime parameters such as stride time, stride distance, and sagittal angles, whose results are compared to RGB-D devices. In [9], OpenPose is used to perform body tracking with a webcam with near real-time gait feedback.

This paper proposes combining the pose estimation models OpenPose and PoseNet with artificial intelligence methods to generate space-time parameters of the gait. Two pathological gaits, namely, hemiparetic and paraparetic, are analyzed in contrast to the gait of a healthy person. The acquisition of images for the pose estimation uses simple mobile phone cameras, which reduces complexity in hardware and allows the use of the proposed system as a remote tool for guiding the treatment of pathological gaits. Experimental results show high accuracy in characterizing and classifying the three gait models.

#### 2. Important Definitions.

- 2.1. **Normal gait.** Bipedal locomotion caused by the displacement of the body segments and characterized by a succession of double and single supports (bipodal and monopodal). During walking, there is a continuous loss and recovery of balance, with a constant movement of the base of support towards the center of gravity.
- 2.2. **Hemiparetic gait.** This gait is a consequence of unilateral injury of the motor cortex. There is a decrease in speed, cadence, and stride length. It is spatially and temporally asymmetric and tends to have equilibrium reactions with higher latencies. The arm on the affected side does not swing, and the leg draws a semicircle with each step, causing alterations in the extension of the lower body joints [10].
- 2.3. **Paraparetic gait.** In this gait, the legs are usually slightly bent at the hip and in the adduction position. The knees are extended, and the feet are plantar flexed. This posture requires circumduction of the legs when walking, forming circles towards the outside of the body. As a result, the march may seem insecure, and slow [11].
- 2.4. **Gait biomechanics.** The study of the biomechanics of gait includes kinematics, which describes movements, and kinetics, which studies the forces that produce movements. In addition, there are various methods for gait analysis, such as digital goniometry, 2D and 3D analysis systems, electromyography, accelerometry, and baropodometry [12]. Figure 1 shows the angular biomechanics of the articulations in a gait cycle.

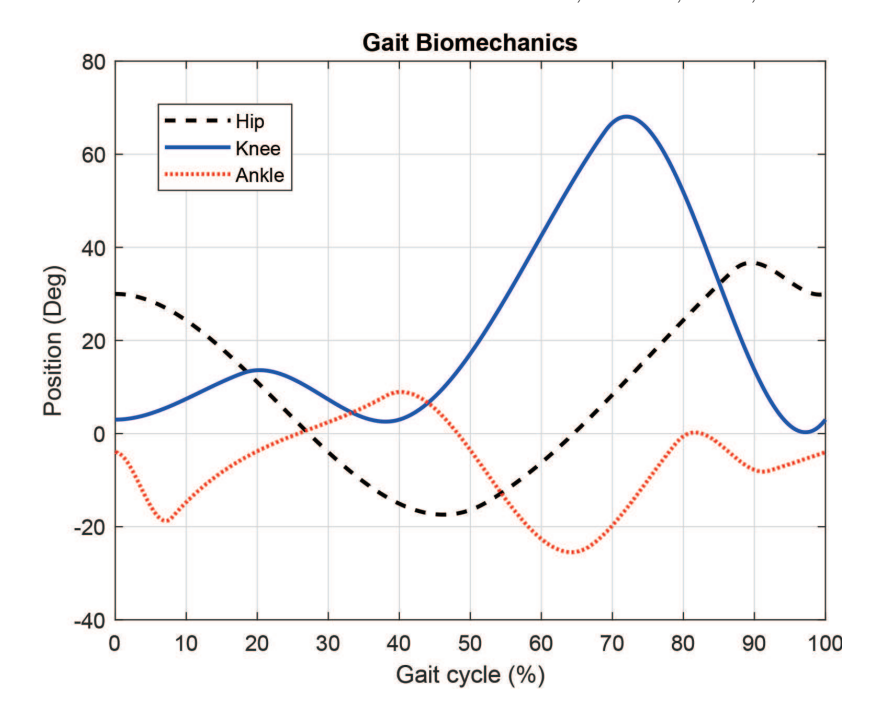


FIGURE 1. Nonpathologic gait biomechanics of the hip, knee, and ankle joints

## 3. Methodology.

3.1. Data acquisition. At the date of development of this work and under the authors' best judgment, a relevant database was not found for the analysis and recognition of normal, hemiparetic, or paraparhetic gaits captured by an RGB camera. Therefore, similar to other works, such as those cited in the literary review, we decided to create our database. Gait trajectories are acquired in an environment with sufficient artificial light and no obstacles. Figure 2 shows the dimensions of a place for capturing the videos, whose measures are 7.15 m long by 4.5 m wide. Two cell phone cameras are placed on tripods at the height of 1.27 m from the side of the sagittal plane and in front of the test subject. The camera's configuration is 720p resolution at 30 frames per second. This setup guarantees that the two planes, sagittal and frontal, can capture the entire body of the person and the most significant amount of information about the gait.

The march is performed starting with the right foot, and the subject completes two cycles. A total of 15 volunteers (nine men and six women) in the range of 20-50 years old

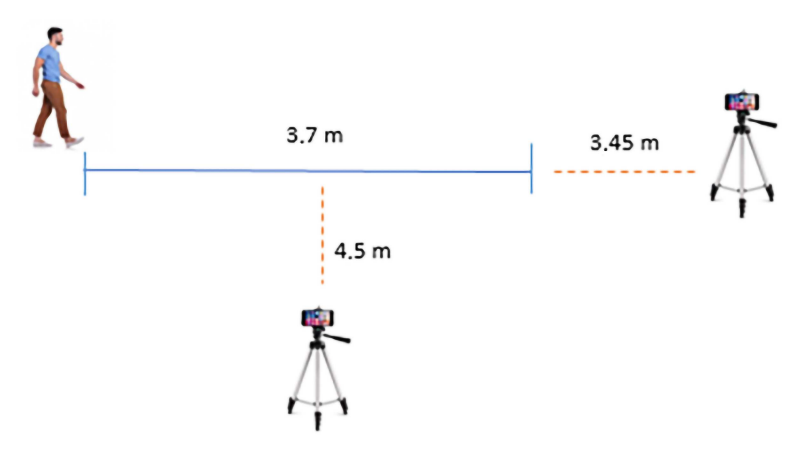


FIGURE 2. Environment setup for data acquisition

were instructed by qualified medical personnel to simulate four sequences of each march. A total of 720 videos were collected, 48 videos per person.

3.2. **Data pre-processing.** After acquiring the videos, we pre-processed them to generate space-time parameters. The analysis of these parameters generates the gait kinematics. Additionally, the march is characterized and classified by a 2D image processing system, which performs digital goniometry by applying the following techniques: video trimming, synchronization, pose estimation, filtering, normalization, and detection of the gait cycle. Figure 3 shows a block diagram of this process.

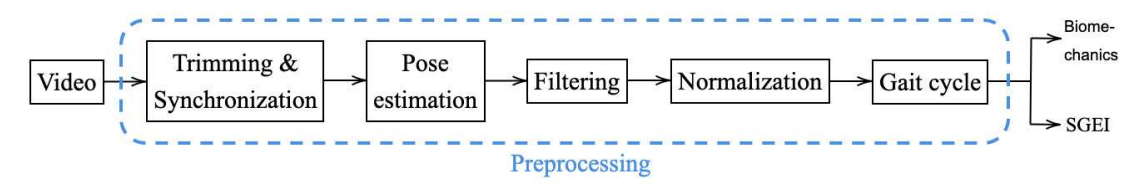


FIGURE 3. Block diagram of the data pre-processing

The trimming-and-sync process delivers videos containing two gait cycles. First, sagittal and frontal plane videos are synchronized by using their audio waveform. This step reduces the processing time in the pose extraction stage and identifies the beginning and end of the gait cycles in the two planes.

The human pose estimation gets the location and orientation of the joints and limbs of the human body in an image. The detected body parts are reported as 2D coordinates of skeletal joints [13]. The pose estimation models OpenPose and PoseNet take the trimmed and synced videos as input and return a set of 25 and 17 2D coordinates for each video frame, respectively.

Once the set of coordinates of each video frame has been obtained, the OpenCV library from [14] is used to draw and join the 2D coordinates. The coordinates of each key point of the body are connected to form a digital skeleton. Figure 4(b) shows how digital skeletons are generated in the sagittal and frontal plane of a person, while walking.

The pose estimation models OpenPose and PoseNet present certain variations among their estimations. Generally, these deviations correspond to minimal errors that can be suppressed or filtered using interpolation functions and a Hanning window. The interpolation covers the gaps, while the Hanning window, shown in Figure 4(c), loops through

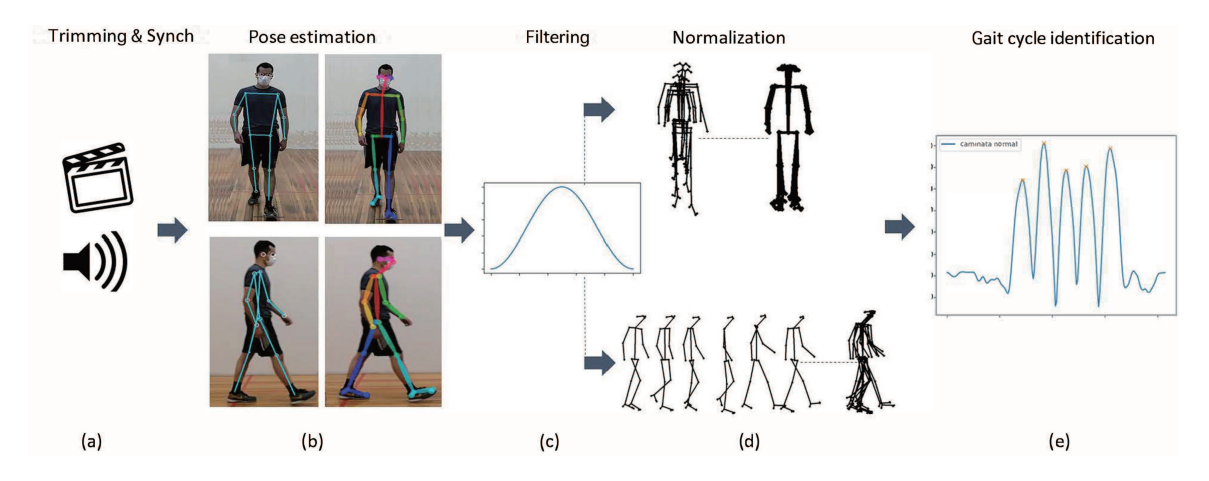


FIGURE 4. General description of the data pre-processing: (a) Trimming and synchronization; (b) pose estimation; (c) filtering; (d) nomalization; (e) gait cycles identification

the set of coordinates of the key points of the body and smooths them. This process allows the measurement error of a pose to be significantly minimized.

After finishing the previous stage, the problem produced by using RGB cameras in a frontal plane must be solved: the size of the digital skeleton increases as the subject walks toward the camera. In [15] a procedure is proposed to mitigate this difficulty and to characterize the digital skeleton independent of the position in which it is found. This approach is used in this work, which implies normalizing the position of the skeleton according to

 $S_{s,w,t} = \frac{dist\left\{ \left( x_{s,w,t}^2, y_{s,w,t}^2 \right), \left( x_{s,w,t}^3, y_{s,w,t}^3 \right) \right\}}{100}$  (1)

$$\hat{P}_{s,w,t}^{n} = \left(\frac{x_{s,w,t}^{n}, x_{s,w,t}^{1}}{S_{s,w,t}}, \frac{y_{s,w,t}^{n}, y_{s,w,t}^{1}}{S_{s,w,t}}\right) = \left(\hat{x}_{s,w,t}^{n}, \hat{y}_{s,w,t}^{n}\right)$$
(2)

where dist(A, B) is the Euclidean distance between the points A and B,  $S_{s,w,t}$  is a scale factor at 100 pixels and  $\hat{P}_{s,w,t}^n$  is the relative position of each point on the skeleton,  $x_{s,w,t}$  and  $y_{s,w,t}$  are the Cartesian coordinates expressed in pixels for each 2D-coordinate of the digital skeleton.

As a result, the skeleton gives the impression of walking on its own ground. Although this problem does not occur in the sagittal plane, the information in this plane must also be normalized to gain consistency in the data. Figure 4(d) shows the skeleton with frontal and sagittal planes of some frames of the gait with and without normalization.

Finally, to generate the space-time parameters and characterize the gait, it is necessary to identify each gait cycle. The gait cycle consists of two periods, one for support and the other for oscillation. The support period corresponds to when the foot is in contact with the ground. In contrast, the period of oscillation is the moment when the foot remains in the air and advances with unipodal support.

To identify the gait cycles, it is drawn the Euclidean distance between the right and left ankle vs. frames per second [16]. Figure 4(e) shows the gait cycle, where each peak represents the maximum distance between the ankles. The first peak is the initial contact, the second peak is the final phase of support, and the third peak corresponds to the final oscillation phase. The graph indicates a total of five peaks, representing two gait cycles.

3.3. Gait characterization by using SGEI. The gait characterization uses a variant of GEI [7]. This method is based on the movement of the binary silhouettes of a pose. This work focuses on obtaining an image with similar characteristics, but instead of body silhouettes, skeleton silhouettes called skeleton gait energy image (SGEI) are generated. Before calculating these images, the skeleton movements are automatically cut out using a bounding box. Taking the midpoint of the hip as the center, the image height and width are resized to  $224 \times 224$  pixels. Finally, the following expression is applied:

$$GEI = \frac{1}{a+N} \sum_{t=a}^{N} I_t(x,y)$$
(3)

where a represents the first frame, N the total number of frames for each cycle of the march, and  $I_t$  the binary skeletal images.

An example of an image containing a complete gait cycle using the OpenPose model and its corresponding SGEI is shown in Figure 5. The SGEI allows a compact representation of the movement throughout a gait cycle. Furthermore, it focuses on the movement of the sequences, which allows a better description of different types of gait. The same procedure is applied to the PoseNet model.

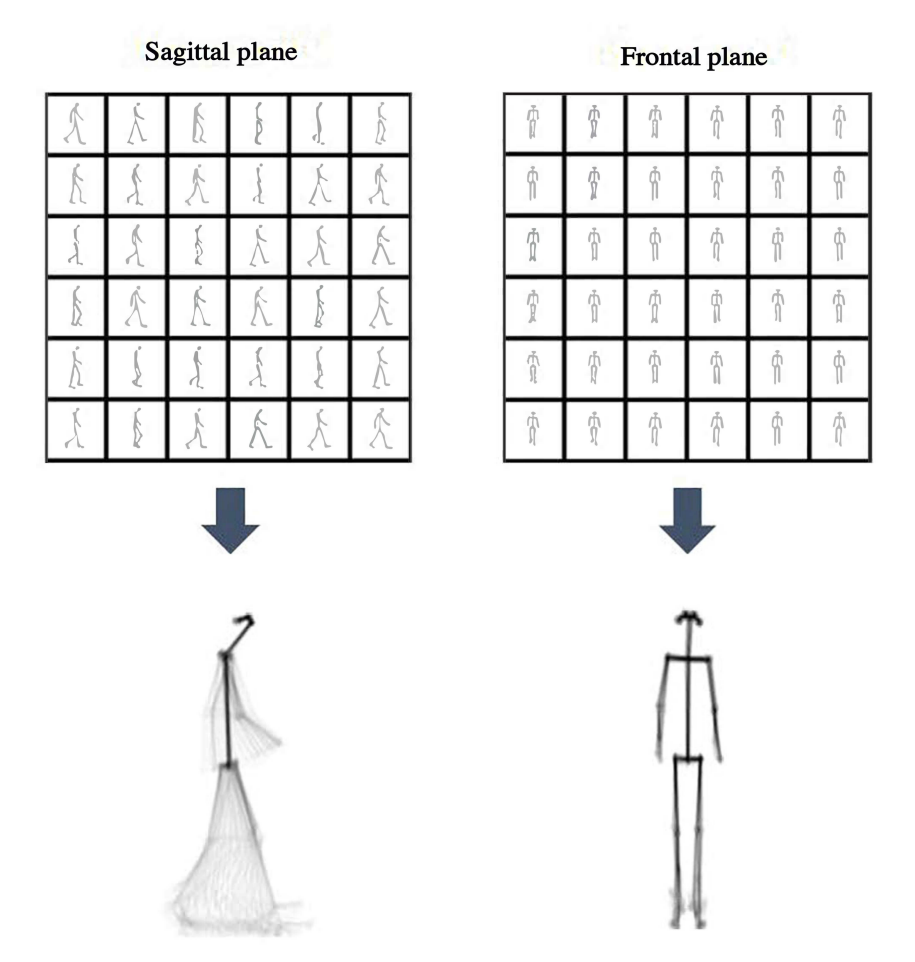


FIGURE 5. SGEI calculation after pose estimation by OpenPose

3.4. Biomechanics calculation. There are several methods for studying gait; this work focuses on kinematics, which describes the movements produced by the human body. Certain space-time parameters are of primary interest and are used to generate the biomechanics of the movement of the lower limbs of normal, hemiparetic, and paraparetic gaits. In addition, parameters used in the clinical evaluation are calculated: stride length, cadence, stride width, stride time, gait speed, angles of the joints of the lower limbs, and inclination of the frontal body posture.

To analyze the three gait patterns, digital goniometry is used, which measures the instantaneous joint's angular position. The 2D analysis allows digitizing the human body as a system of points linked by segments. Using the coordinates of the key points obtained as output from the PoseNet and OpenPose models, the angles of the lower limb joints are calculated for each frame of a gait cycle. Figure 6 and Table 1 show these angles in the sagittal and frontal planes, along with their corresponding label.

3.5. Features extraction and classification. The first approach for classifying the three gait patterns under study is convolutional neural networks (CNN) due to their simplicity for training and deployment. Figure 7 shows the VGG19 architecture [17] used. The input image dimensions are  $224 \times 224 \times 3$  pixels. Two convolutional layers of 64 kernels of  $3 \times 3$  each are applied to detecting certain characteristics of the original image. A max-pooling layer is used to halve the neurons generated in previous layers. The first few layers detect basic shapes, such as edges and curves. The convolutions applied with the 128, 256, and 512 kernels in subsequent layers detect more complex structures in the

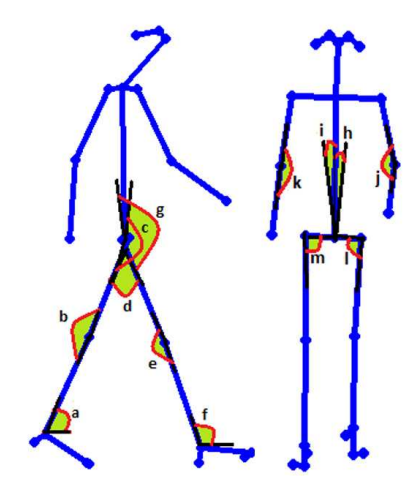


Figure 6. Joint angles description

Table 1. Labels and description of joint angles

ID	Joint angle	ID	Joint angle	ID	Joint angle	ID	Joint angle
a	Right ankle	d	Sagittal	g	Left hip	j	Left elbow
b	Right knee	e	Left knee	h	Left body inclination	k	Right elbow
c	Right hip	f	Left ankle	i	Right body inclination	1	Left front hip



FIGURE 7. VGG19 architecture applied to gait classification

image [6]. Flattening is added; it is no longer a three-dimensional problem. Additionally, a function called *softmax* is applied in the final output layer, which has the number of neurons corresponding to the classes being classified, that is, the three classes of gaits: normal, hemiparetic, and paraparetic.

The input of the CNN corresponds to the SGEI images. Since our database is small, it is impractical to retrain all layers due to possible problems with overtraining. Consequently, we use the learning transfer method. The architecture weights are reused, and only the last fully connected layer is trained, which is in charge of the classification.

A second approach for classification implies using the space-time parameters of Table 2. A total of 28 variables make up a vector of gait characteristics, including maximum and minimum values. Additionally, vector parameters are averaged for each gait cycle. SVM is chosen as the classification algorithm since the input is no longer an image but a data set. Additionally, SVM is memory efficient, and as shown in [2], it is applicable for gait characterization. SVM belongs to the category of linear classifiers that induce linear separators. If these are not linearly separable, kernel functions are used [18]. Linear kernel functions are a specific case of the kernel radial base function (RBF), which is nonlinear and, contrary to the linear kernel, can handle nonlinear relationships between classes and their attributes, as is the case of this work. The SVM used in this work has the RBF

Max angle left ankle (°)

Min angle left ankle (°)

 $94.26 \pm 7.80$ 

 $55.27 \pm 7.14$ 

Space time personators	OpenPose			PoseNet			
Space-time parameters	Hemiparetic	Normal	Paraparetic	Hemiparetic	Normal	Paraparetic	
Right step length (m)	$0.34 \pm 0.05$	$0.52 \pm 0.06$	$0.32 \pm 0.08$	$0.32 \pm 0.05$	$0.50 \pm 0.06$	$0.31 \pm 0.08$	
Left step length (m)	$0.24 \pm 0.07$	$0.53 \pm 0.07$	$0.29 \pm 0.08$	$0.24 \pm 0.07$	$0.49 \pm 0.06$	$0.28 \pm 0.08$	
Right stride length (m)	$0.58 \pm 0.10$	$1.04 \pm 0.13$	$0.60 \pm 0.14$	$0.56 \pm 0.09$	$0.99 \pm 0.10$	$0.57 \pm 0.13$	
Left stride length (m)	$0.58 \pm 0.10$	$1.06 \pm 0.12$	$0.60 \pm 0.14$	$0.56 \pm 0.09$	$1.00 \pm 0.10$	$0.58 \pm 0.13$	
Step amplitude (m)	$0.25 \pm 0.05$	$0.15 \pm 0.08$	$0.32 \pm 0.08$	$0.27 \pm 0.05$	$0.16 \pm 0.03$	$0.36 \pm 0.08$	
Step time (s)	$0.79 \pm 0.12$	$0.61 \pm 0.04$	$1.01 \pm 0.30$	$0.78 \pm 0.12$	$0.62 \pm 0.05$	$1.01 \pm 0.30$	
Walking speed (m/s)	$0.44 \pm 0.14$	$1.14 \pm 0.16$	$0.36 \pm 0.10$	$0.43 \pm 0.14$	$1.15 \pm 0.17$	$0.36 \pm 0.10$	
Cadency (steps/min)	$77.73 \pm 11.27$	$98.17 \pm 6.67$	$64.22\pm17.01$	$78.58 \pm 12.28$	$97.88 \pm 7.02$	$64.77\pm18.24$	
Right sagittal angle (°)	$25.68 \pm 6.73$	$39.42 \pm 9.41$	$27.69 \pm 7.70$	$24.65 \pm 6.05$	$40.05 \pm 7.18$	$25.38 \pm 7.82$	
Left sagittal angle (°)	$25.74 \pm 8.85$	$38.36 \pm 9.80$	$24.17 \pm 8.38$	$25.95 \pm 8.88$	$37.98 \pm 7.21$	$23.64 \pm 8.67$	
Right inclination (°)	$5.37 \pm 3.91$	$2.88 \pm 1.43$	$9.83 \pm 4.18$	$5.54 \pm 4.16$	$3.50 \pm 1.98$	$9.84 \pm 4.06$	
Left inclination (°)	$10.67 \pm 3.99$	$3.84 \pm 2.05$	$10.92 \pm 4.41$	$11.13 \pm 4.38$	$4.36 \pm 1.56$	$11.17 \pm 4.67$	
Max front angle right hip (°)	$96.43 \pm 3.00$	$90.68 \pm 2.21$	$99.64 \pm 3.63$	$104.073 \pm 5.00$	$96.73 \pm 7.71$	$107.37\pm6.44$	
Max front angle left hip (°)	$97.61 \pm 3.18$	$91.75 \pm 2.68$	$99.95 \pm 3.75$	$108.60 \pm 7.03$	$97.07 \pm 11.15$	$105.90\pm5.87$	
Max angle right knee (°)	$182.59 \pm 3.26$	$181.14 \pm 12.43$	$182.36\pm3.81$	$180.99 \pm 3.47$	$177.37 \pm 3.79$	$181.76\pm4.08$	
Min angle right knee (°)	$169.46 \pm 7.08$	$124.17 \pm 14.44$	$164.17\pm6.12$	$166.63 \pm 7.18$	$124.59 \pm 6.63$	$162.18 \pm 6.51$	
Max angle right hip (°)	$186.09 \pm 6.33$	$191.37 \pm 5.65$	$187.66\pm7.57$	$185.13 \pm 6.04$	$191.65 \pm 5.62$	$187.59 \pm 6.44$	
Min angle right hip (°)	$167.10 \pm 8.92$	$158.77 \pm 3.93$	$164.44 \pm 8.09$	$164.90 \pm 8.50$	$157.52 \pm 3.37$	$164.02 \pm 7.25$	
Max angle right ankle (°)	$102.51 \pm 4.65$	$109.61 \pm 6.99$	$98.39 \pm 5.72$	$101.98 \pm 5.69$	$107.31 \pm 4.47$	$98.02 \pm 5.66$	
Min angle right ankle (°)	$74.54 \pm 7.12$	$43.61 \pm 7.79$	$65.67 \pm 5.12$	$72.60 \pm 6.82$	$44.56 \pm 4.81$	$64.25 \pm 5.49$	
Max angle left knee (°)	$178.80 \pm 9.04$	$180.83 \pm 12.34$	$181.51\pm6.12$	$177.29 \pm 4.40$	$176.78 \pm 3.50$	$180.76 \pm 5.66$	
Min angle left knee (°)	$139.58 \pm 12.90$	$127.22 \pm 14.36$	$158.21\pm9.25$	$140.2 \pm 9.81$	$126.10 \pm 7.15$	$156.75 \pm 8.16$	
Max angle left hip (°)	$188.39\pm7.23$	$192.72 \pm 5.09$	$188.83\pm6.43$	$190.28 \pm 5.98$	$195.00 \pm 5.59$	$190.18\pm6.01$	
Min angle left hip (°)	$161.35 \pm 7.62$	$160.65 \pm 3.63$	$165.48 \pm 7.14$	$160.97 \pm 7.54$	$159.87 \pm 4.77$	$165.15 \pm 7.17$	

Table 2. Space-time parameters of the gait for OpenPose and PoseNet models

kernel to classify the three classes of gaits with input from a data vector made up of 28 space-time parameter variables.

 $43.52 \pm 8.04$   $61.35 \pm 5.44$ 

 $109.65 \pm 6.98$   $96.79 \pm 6.38$   $92.62 \pm 5.67$   $109.29 \pm 5.70$   $95.63 \pm 6.40$ 

 $55.54 \pm 5.16$   $43.10 \pm 4.88$   $60.08 \pm 5.60$ 

- 4. **Results.** Experimental data is processed on a personal computer with an IntelCore i7-5th generation CPU, 8 GB of RAM, and a 2 GB Nvidia GeForce 760 graphics card. Additionally, GPU-oriented cloud computing from Google Colab is used to reduce the execution time in the preprocessing and training stages. Finally, about 7%-8% of the total information processed is discarded because the models present variations in the pose estimates when a person dresses in black clothing.
- 4.1. Space-time parameters and digital goniometry. Table 2 shows average values of the space-time parameters as well as their standard deviations. The OpenPose and PoseNet models provide this information by analyzing RGB videos of 15 volunteers who perform normal, hemiparetic, and paraparetic gaits. The results synthesize the analysis of the mobility of the lower right (R) and left (L) limbs.

The results of cadence (98.17 steps/min) and gait speed (1.14  $\pm$  0.16 m/s) corresponding to normal gait are similar to the results of [19] (cadence of 103.5 steps/min and speed range of 1.2 to 1.4 m/s), where eight volunteers without gait disorders (four women and four men) aged 21-28 years were evaluated. In addition, [20] obtains an average step time of 0.61  $\pm$  0.04 m/s over a sample of 236 healthy adult patients. This result is identical to the value shown in Table 2.

In work developed by [21] it is estimated a stride length of  $0.55 \pm 0.065$  m for Kuwaiti men and women aged 20-29 years. Our work obtains a stride length of  $0.53 \pm 0.07$  m. The stride length ( $0.15 \pm 0.08$  cm) calculated in this work is similar to the one reported in [22], whose results are  $13.7 \pm 3.3$  cm for men's stride length, and  $9.9 \pm 1.4$  cm for women's stride length, for a total of 18 subjects.

As previously discussed, our results are concordant with the previous investigations, which generate confidence in the post-processing of the information to calculate other parameters, such as the biomechanics of gait.

The values of stride length of normal gait (R=0.52 m) (L=0.53 m) as well as the inclination of the body  $(R=2.88^{\circ}, L=3.84^{\circ})$  for both legs are similar, which indicates that the body remains stable and the steps for each leg are relatively equal to each other. The walking speed and cadence values show that normal gait is faster than the other two gait patterns, implying a journey with fewer steps for the same distance. Furthermore, the minimum angles of the hip  $(R=158.77^{\circ}, L=160.65^{\circ})$ , knee  $(R=124.17^{\circ}, L=127.22^{\circ})$ , and ankle  $(R=43.61^{\circ})$   $(L=43.52^{\circ})$ , show that there is a greater deflection in the initial phase of oscillation compared to the other two gaits. It is important to consider that the participants' height impacts the results.

Hemiparetic gait is spatially and temporarily asymmetric, as demonstrated by the parameter of inclination to the right and the left with values of  $5.37^{\circ}$  and  $10.67^{\circ}$ , respectively. The stride length parameter ( $R=0.32~\mathrm{m},\ L=0.24~\mathrm{m}$ ) indicates that the right leg takes a larger step than the left leg.

It also can be seen, from Table 2, that the body inclination during hemiparetic gait  $(R = 5.54^{\circ}, L = 11.13^{\circ})$  is bent to the left. Additionally, the minimum flexion values produced by the knee  $(R = 166.63^{\circ}, L = 140.2^{\circ})$  indicate an asymmetry since the right leg draws a semicircle causing excessive inclination to one side, denoting that the condition is in the right part of the body.

The paraparetic gait is rigid and insecure; this is demonstrated by the results of parameters that are very characteristic of this pathology, such as the walking speed (0.36 m/s), walking time (1.01 s), and cadence (64.22 steps/min) that are lower compared to normal or hemiparetic gaits. The body inclination ( $R = 9.83^{\circ}$ ,  $L = 10.92^{\circ}$ ) reveals that the alteration in the walk and the affection is present in both legs.

The space-time parameters obtained using PoseNet show that the average values differ by 2.98% regarding the OpenPose model. This evidence indicates a minimal divergence between the results of the two models.

The gait biomechanics models correspond to Cartesian graphs that relate the joint angle vs. % gait cycle. These representations are obtained from the OpenPose and PoseNet models, extracted from the flexion carried out in sagittal view by the hip, knee, and right ankle

Figure 8 shows the flexion performed by the right hip and the patterns generated from the three gait patterns. The green region represents the angle variations produced by the 15 volunteers. Figures 9 and 10 show the flexion performed by the knee and the ankle, respectively. Only the angular positions of the right sagittal plane are evaluated since

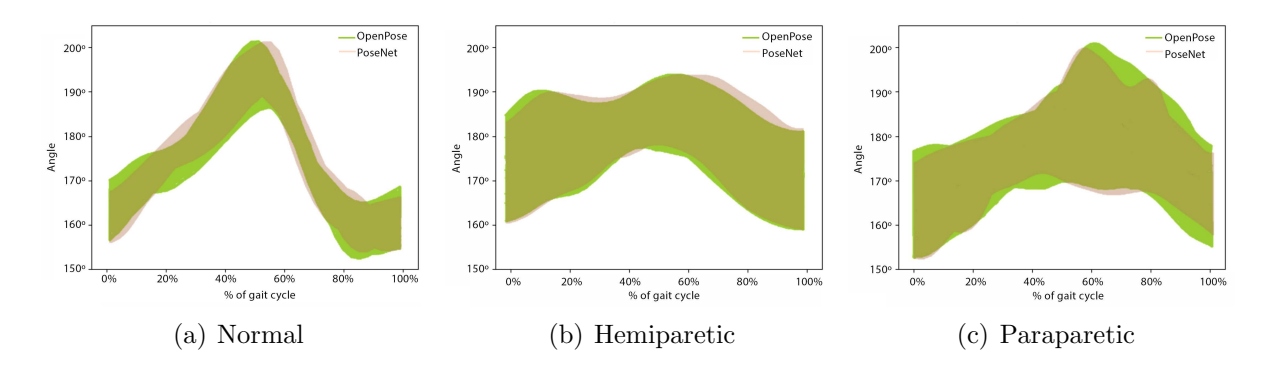


FIGURE 8. (color online) Hip joint angular displacement vs. % gait cycle

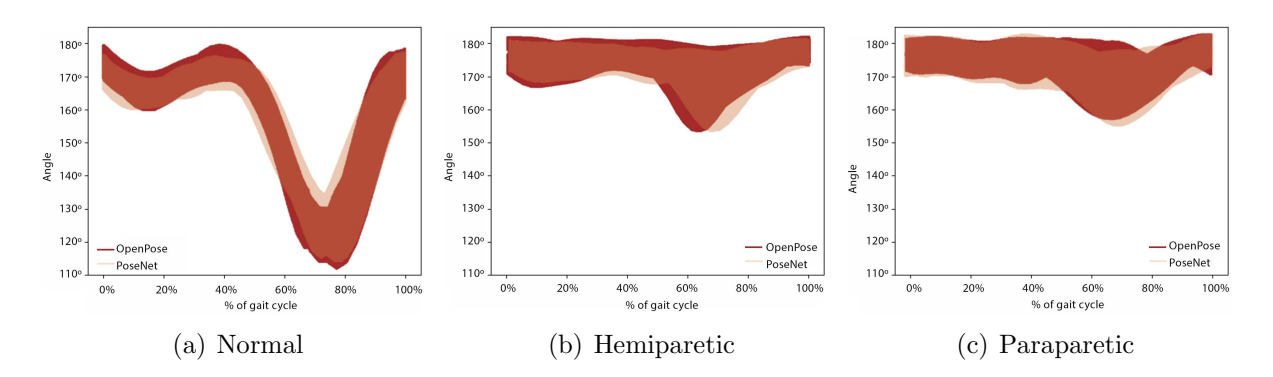


FIGURE 9. (color online) Knee joint angular displacement vs. % gait cycle

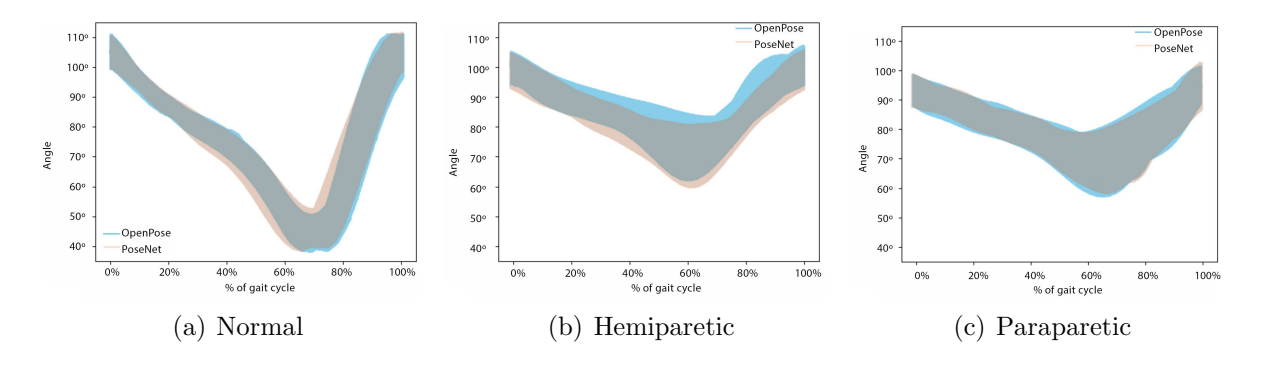


FIGURE 10. (color online) Ankle joint angular displacement vs. % gait cycle

the left side is an inverted mirror of the right side, except for the hemiparetic gait. The patterns of lower body joint movements in normal gait are consistent with those analyzed in [23].

The differences between the normal gait pattern and the pathological ones are noticeable; both the stance phase (60% of the cycle) and the oscillation phase (40% remaining) are altered. Figure 8 additionally illustrates that in 50% of the normal gait cycle, there is a more defined peak with a maximum value of 200° while, in the hemiparetic gait, the pattern is flatter; in the paraparetic gait, the peak shifts to 65% of the cycles and its margins start at 150°.

Figure 9 shows a well-defined pattern in the articular angles of the knee that corresponds to normal gait. A 15% of the cycle corresponds to the damping phase, that is, the weight of the body is supported on the right leg, causing a slight flexion, while from 60% to 90% of the cycle starts the oscillation stage, where the leg is in the air, and the knee performs its maximum flexion. The last 10% corresponds to the final swing phase, with the leg returning to its initial support state. In both hemiparetic and paraparetic gait, the results show patterns with a tendency to be flat, except in 65% of the gait cycle, where the knee flexion is slight.

Figure 10 shows the pattern generated by the ankle angle. The maximum value of this joint is  $40^{\circ}$  and occurs between 60% and 80% for normal gait, forming a V-shaped pattern. On the other hand, the other two marches show a flattened flex with a peak of approximately  $60^{\circ}$  and only differentiated by a minor alteration in 90% of the hemiparetic gait cycle.

- 4.2. Accuracy of the classifiers. The results of the performance of the CNN and SVM classification algorithms with the OpenPose and PoseNet models, applied to the three gait patterns, are discussed in this subsection.
- 4.2.1. Parameters adjustment and precision of the CNN. During the adjustment of the training parameters, a maximum batch size of 32 is selected, allowing the model to converge faster. The number of epochs was set to 10, and the loss function was set to categorical cross entropy. The stochastic gradient descent (SGD) optimizer is also used with a learning rate of 0.0002.
  - OpenPose. A total of 2794 SGEI images were obtained using OpenPose, 1138 of the hemiparetic gait, 546 of the normal gait, and 1110 of the paraperetic gait. The training set corresponds to 70% of all samples in every case 15% for validation and the remaining 15% for testing. The classification performance was evaluated using 421 SGEI images (171 hemiparetic, 83 normal, and 167 paraparetic). The confusion matrix and ROC curves are used as evaluation tools for performance comparison. The results of the confusion matrix and the ROC curves are shown in Figures 11(a) and 11(b), respectively. Six samples out of 421 were erroneously classified, which indicates a precision of 98.57% and an area under the curve close to 1.

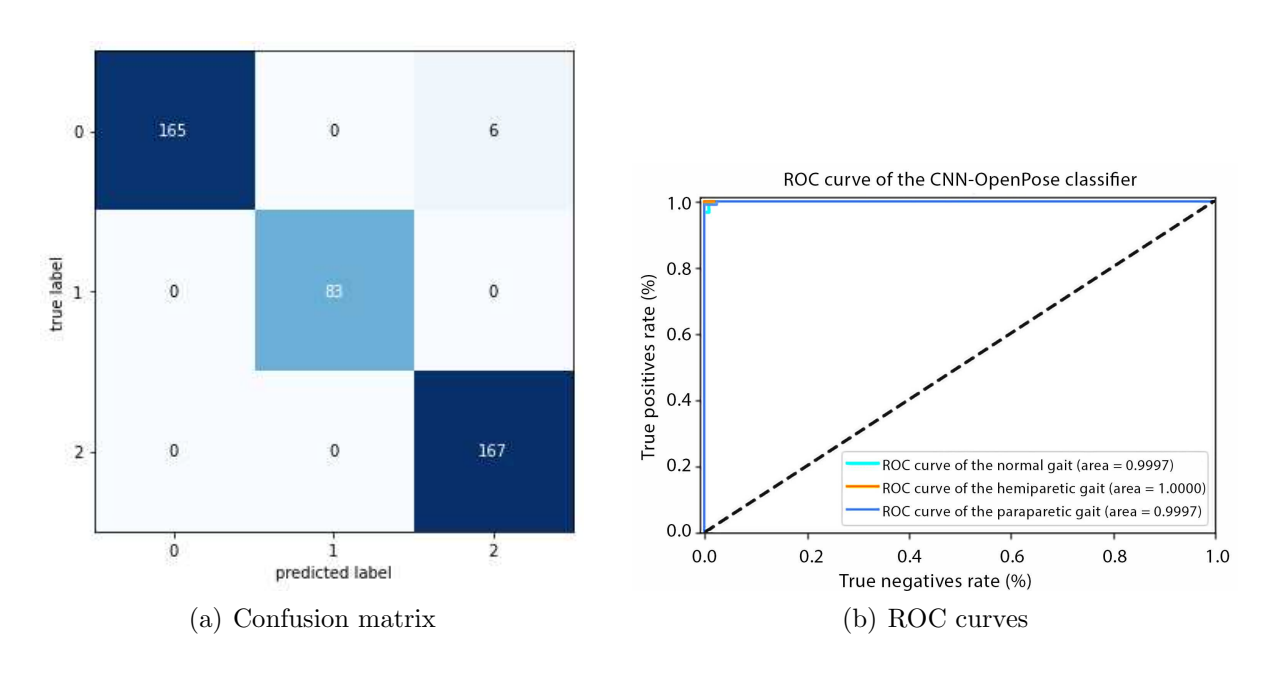


FIGURE 11. Performance of the OpenPose & CNN classifier

• PoseNet. A total of 2880 SGEI images were obtained using PoseNet (3% more than OpenPose since this model is a bit more robust when patients wear black clothing), 1188 from the hemiparetic gait, 544 from the normal gait, and 1148 from the paraparetic gait. The training set corresponds to 70% of all samples in every case, 15% for validation, and the remaining 15% for testing. A set of 433 SGEI images (179 hemiparetic, 82 normal, and 172 paraparhetic) belonging to the three gait patterns were evaluated using a confusion matrix and ROC curves.

The results of the confusion matrix and the ROC curves are shown in Figures 12(a) and 12(b), respectively. Eight samples out of 421 were erroneously detected, indicating a precision of **98.15%**, 0.42% lower than OpenPose.

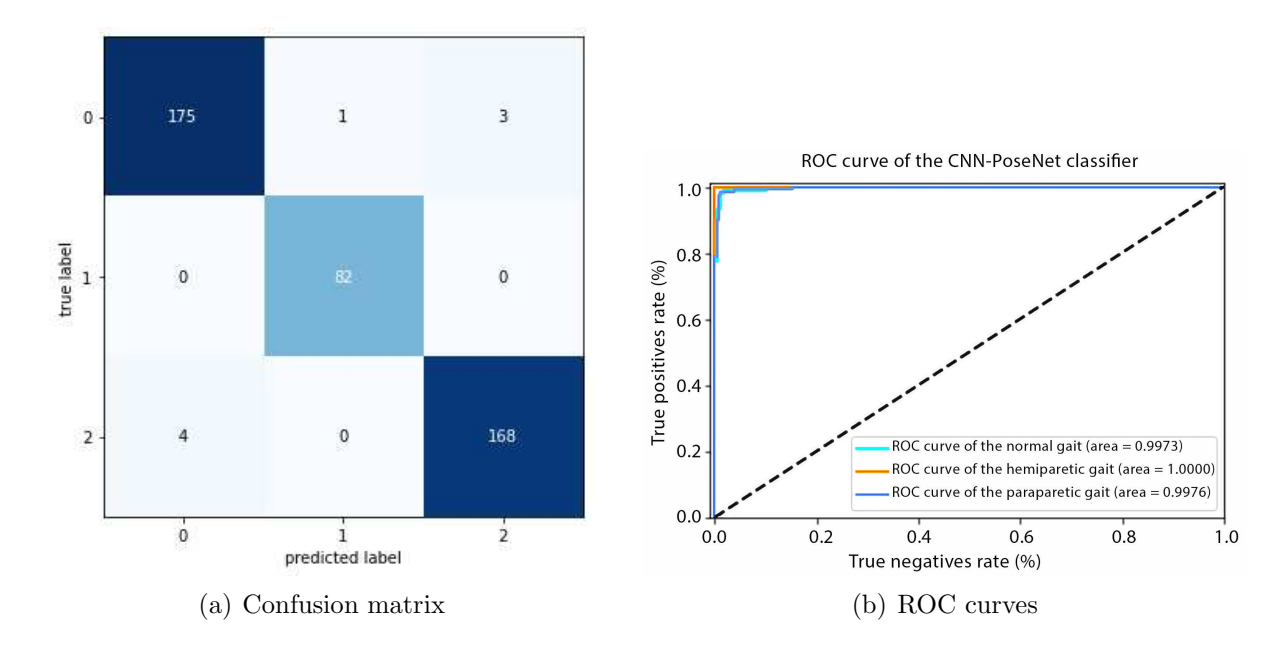


FIGURE 12. Performance of the PoseNet & CNN classifier

- 4.2.2. Parameters adjustment and precision of the SVM. The SVM classification algorithm uses as input the space-time parameters extracted from the 15 participants, obtaining a total of 28 variables for each gait. The SVM algorithm uses the RBF kernel.
  - OpenPose. The data set used for performance evaluation corresponds to 319 data vectors, where 104 belong to the hemiparetic gait, 111 to the normal gait, and 104 to the paraperetic gait. The training set is composed of 70% of the information, while the remaining 30% is used for testing. A set of 96 vectors (36 hemiparetic, 35 normal, and 25 paraparetic) was evaluated by a confusion matrix and ROC curves.

The results of the confusion matrix show that three vectors out of the 96 were detected erroneously, which indicates a precision of **96.87%** and an area under the curve close to **1**, as illustrated in Figure 13. The percentage is 1.7% lower than the SGEI-CNN approach with the OpenPose model.

• PoseNet. The data set used for performance evaluation corresponds to 329 data vectors, where 106 belong to the hemiparetic gait, 111 to the normal gait, and 112 to the paraperetic gait. The training set is composed of 70% of the information, while the remaining 30% is used for testing. Ninety-nine vectors (33 hemiparetic, 31 normal, and 35 paraparetic) were evaluated by a confusion matrix and ROC curves.

The results of the confusion matrix show that five vectors out of the 96 were detected erroneously, which indicates a precision of **94.94%** and an area under the curve close to **1**, as shown in Figure 14. The accuracy percentage is 3.21% lower than the SGEI-CNN approach with the PoseNet model.

4.3. **System limitations.** The proposed system, composed of digital image processing algorithms with pose estimation and machine learning algorithms, requires high computing capabilities for successful data processing. For instance, using the PoseNet model implies using a graphics processor unit (GPU) within the computer. On the other hand, the OpenPose model is less memory-consuming and could be used without a GPU. Furthermore, future improvements in our work imply reducing image processing complexity by using novel approaches for feature extractions, such as image processing through wavelet analysis [24].

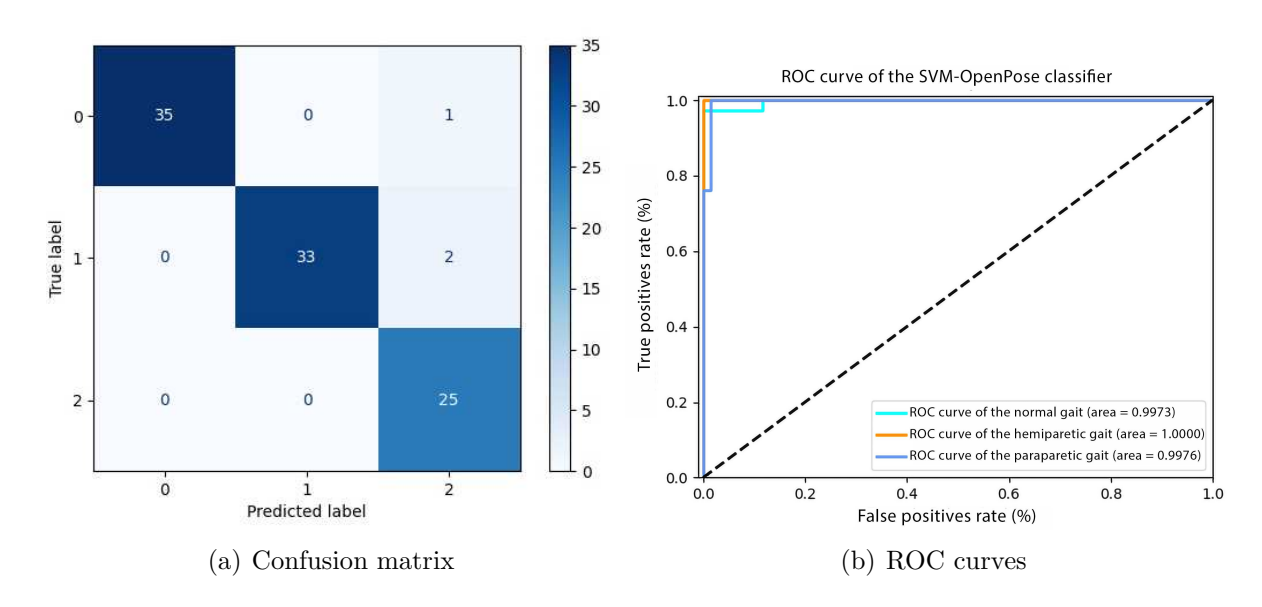


FIGURE 13. Performance of the OpenPose & SVM classifier

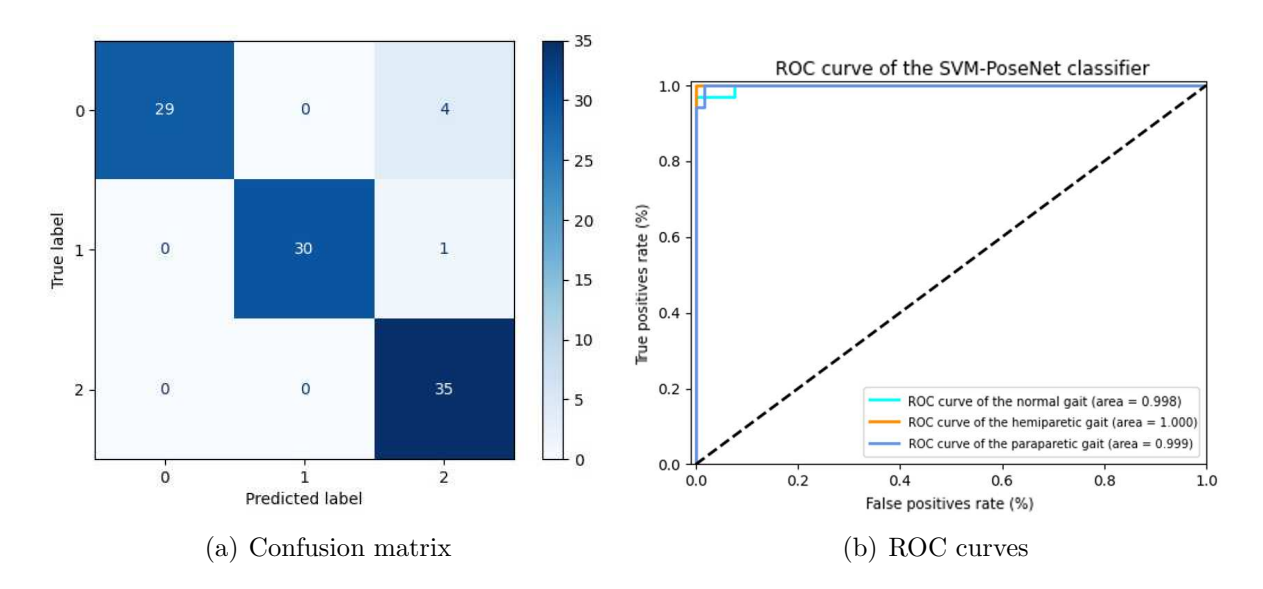


FIGURE 14. Performance of the PoseNet & SVM classifier

The pose models are susceptible to estimation errors when patients dress in black or wear loose clothing. Though this is a drawback of our system, it is a minor problem since an appropriate dress code instruction for patients would be enough.

5. **Conclusions.** The results of the non-invasive system proposed in this work indicate that the space-time parameters and the gait biomechanics obtained are consistent with the foregoing investigations. Therefore, this system can be used as an analysis tool for guiding the treatment of pathological gaits, such as those evaluated in this study.

Gait analysis using non-invasive models such as OpenPose and PoseNet plays a fundamental role in the follow-up of patients who cannot attend a specialized center. In addition, using a video taken by an everyday device such as a cell phone reduces the complexity and inconvenience of other methods and allows a healthcare professional to objectively assess gait disturbances.

In this study, we identify and classify normal, hemiparetic, and paraparhetic gait using data generated from RGB videos and the OpenPose and PoseNet models. The experiments show that the SGEI approach as a method to characterize gait, and the use of a CNN with a variant of the VGG19 architecture, reach a maximum of 98.57% precision. Furthermore, another approach implying 28 space-time variables to characterize gait, together with the SVM algorithm, shows a maximum of 96.87% precision in the classification. The results show a relevant improvement compared to other approaches presented in related works, with reported performances up to 89.6%.

#### REFERENCES

- [1] N. David, P. Chipol, J. Alfonso, B. Fernández, L. Héctor Hernández Gómez, A. González Rebattú, J. Francisco, O. R. Romero, C. Horacio, M. Salguero, N. D. Pava, L. H. Hernández Gómez, J. A. Beltrán Fernández, J. F. Pava Chipol, O. R. Romero, C. H. M. Salguero, A. González and R. Rebatt, Methodology of evaluation of normal and pathological gait by correlating digital images, *Journal de Ciencia e Ingeniería*, vol.10, no.1, pp.39-46, 2018.
- [2] Q. Li, Y. Wang, A. Sharf, Y. Cao, C. Tu, B. Chen and S. Yu, Classification of gait anomalies from Kinect, *The Visual Computer*, no.34, pp.1-13, 2018.
- [3] N. Nobuyasu, S. Tetsuro, U. Kazuhiro, O. Leon, A. Kimura, I. Yoichi, F. Senshi and Y. Shinsuke, Evaluation of 3D markerless motion capture accuracy using OpenPose with multiple video cameras, Frontiers in Sports and Active Living, no.2, 2020.
- [4] P. Gonzalez, Biomechanical Analysis of Gait Using an Analytical Model of Inverse Dynamics in Patients with Alterations in the Sagittal Balance of the Spine, Ph.D. Thesis, Universitat Autònoma de Barcelona, 2017.
- [5] N. Abid, RGB-Depth Based Gait Data Analysis for Asymmetry Detection, Master Thesis, University of Calgary, Calgary, Alberta, 2019.
- [6] J. Santos, *Using Deep Learning for Gait Abnormality Classification*, Master Thesis, Department of Electrical and Computer Engineering, University Lisboa, Lisboa, Portugal, 2019.
- [7] J. Han and B. Bhanu, Individual recognition using gait energy image, IEEE Trans. Pattern Analysis and Machine Intelligence, vol.28, no.2, 2006.
- [8] J. Stenum, C. Rossi and R. Roemmich, Two-dimensional video-based analysis of human gait using pose estimation, *PLoS Computational Biology*, vol.17, no.4, DOI: 10.1371/journal.pcbi.1008935, 2020.
- [9] S. R. Rick, S. Bhaskaran, Y. Sun, S. McEwen and N. Weibel, NeuroPose: Geriatric rehabilitation in the home using a webcam and pose estimation, *Interciencia*, pp.105-106, 2019.
- [10] F. M. Rueda and M. C. Tejada, *Human Gait: Biomechanica, Evalution and Pathologies*, Editorial Médica Panamericana S.A., 2020.
- [11] W. Pirker and R. Katzenschlager, Gait disorders in adults and the elderly: A clinical guide, Wiener Klinische Wochenschrift, no.129, pp.81-95, 2016.
- [12] R. Cano, R. Martinez and J. Miangolarra, Control and motor learning: Fundamentals, development and rehabilitation of the human movement, *Deficiencias del Sistema Motor II. Evaluación de las Alteraciones del Tono Muscular*, 2016.
- [13] M. Pearson, Automatic Gait Recognition, Master Thesis, Linkping University, Linkping, Suecia, 2020.
- [14] Z. Cao, G. Martinez, T. Simon, S. Wei and Y. A. Sheikh, Openpose: Realtime multi-person 2D pose estimation using part affinity fields, *IEEE Trans. Pattern Analysis and Machine Intelligence*, 2019.
- [15] M. Kumar and R. Babu, Human gait recognition using depth camera: A covariance based approach, Proc. of the 8th Indian Conference on Computer Vision, Graphics and Image Processing, 2012.
- [16] G. Garcia and G. Gonzalez, Recognition of Fingerprint Images by Means of the Daubechies Wavelet Transform and Euclidean Distances, Master Thesis, Instituto Politécnico Nacional, México DF, México, 2015.
- [17] K. Simonyan and A. Zisserman, Very deep convolutional networks for large-scale image recognition, arXiv.org, arXiv: 1409.1556, 2014.
- [18] E. J. Carmona, *Tutorial of Support Vector Machines (SVM)*, Universidad Nacional de Educación a Distancia (UNED), Madrid, Spain, 2016.
- [19] Y. N. Stephania, Comparative Study of Gait Analysis Systems Based on Inertial Sensors and Infrared Cameras, Master Thesis, Universidad de Concepción, Concepción, Chile, 2018.

- [20] T. Diana, C. Andrea, P. Elisa, A. Laura, M. Anat, M. H. Jeffrey and C. U. Della, Estimation of step-by-step spatio-temporal parameters of normal and impaired gait using shank-mounted magneto-inertial sensors: Application to elderly, hemiparetic, parkinsonian and choreic gait, *Journal of Neuro Engineering and Rehabilitation*, 2014.
- [21] A.-O. Saud, W. James, A.-Y. Alia and A.-G. Muneera, Basic gait parameters: A comparison of reference data for normal subjects 20 to 29 years of age from Kuwait and Scandinavia, *Rehabilitation Research & Development*, no.4, 2003.
- [22] P. Grabiner and S. Biswas, Age-related changes in spatial and temporal gait variables, *Arch. Phys. Med. Rehabil.*, pp.31-35, 2001.
- [23] F. Multon, G. Nicolas, R. Crompton, K. D'Août and G. Berillon, Anthropometry in bipedal locomotion: The link between anatomy and gait, *Handbook of Anthropometry: Physical Measures of Human Form in Health and Disease*, 2012.
- [24] Y. Zhao and Q. Huang, Image enhancement of robot welding seam based on wavelet transform and contrast guidance, *International Journal of Innovative Computing*, *Information and Control*, vol.18, no.1, pp.149-159, 2022.

### **Author Biography**



Stalin Benenaula received a bachelor's degree in electronic engineering from Universidad de Cuenca, Ecuador, in 2021. Currently, he works at CEDIA in the networking operation center. His research interests include artificial intelligence applied in health and biomedicine.



Milton Damian Trelles received a bachelor's degree in electronic engineering from Universidad de Cuenca, Ecuador, in 2021. He has recently worked in the field of electromedicine in some health centers in the south of Ecuador. His research interests include artificial intelligence applied in health and biomedicine.



Luis Eduardo Garza-Castañón received the Engineering degree in Electronic Systems, the M.Sc. degree in control engineering, and the Ph.D. in artificial intelligence from Tecnologico de Monterrey, Monterrey, Mexico, in 1986, 1988, and 2001, respectively. From 1999 to 2003, he was a Lecturer with the Tecnologico de Monterrey Physics Department. Since 2004, he has been an Associate Professor with the Mechatronics Department, Tecnologico de Monterrey, Campus Monterrey. He is the author of more than 100 articles, chapter books, and books. His research interests include fault-tolerant control, industrial processes optimization, and robotics.



Luis Ismael Minchala received his B.S.E.E. degree in 2006 from the Salesian Polytechnic University, Ecuador, and his M.Sc. and Ph.D. degrees from Tecnologico de Monterrey, Mexico, in 2011 and 2014, respectively. From summer 2012 to summer 2013, he was a visiting scholar at Concordia University in Montreal, Canada. Between 2017-2018 he was a Postdoctoral Fellow at Tecnologico de Monterrey in the Climate Change Research Group. Dr. Minchala has authored over 60 indexed publications, including journal articles, conference proceedings, book chapters, and a book. His research interests include applied control engineering, fault-tolerant control, microgris, wind energy and wind turbines control.